

## PHYSICO-CHEMICAL PROPERTIES OF NANO-SIZED HEXAGONAL HYDROXYAPATITE POWDER SYNTHESIZED BY SOL-GEL

A. COSTESCU, I. PASUK, F. UNGUREANU, A. DINISCHIOTU<sup>a</sup>, M. COSTACHE<sup>a</sup>, F. HUNEAU<sup>b</sup>, S. GALAUP<sup>c</sup>, P. LE COUSTOMER<sup>b</sup>, D. PREDOI<sup>\*</sup>  
*National Institute of Materials Physics, P.O. box MG-7, Bucharest-Magurele, Ilfov, 077125, Romania,*

<sup>a</sup>*Molecular Biology Center, University of Bucharest, 91-95 Splaiul Independenței, 76201, Bucharest 5, Romania*

<sup>b</sup>*Universite Bordeaux 1, Avenue des Facultés, Bat 18, 33405 Talence Cedex France,*

<sup>c</sup>*IUT Michel de Montaigne –Bordeaux 3, 1 rue Jacques Ellul 33080 Bordeaux cedex France,*

Calcium phosphate ceramic powders were synthesized via sol-gel method. The powders were sintered at 600 and 1000°C and characterized by X-ray diffraction (XRD), X-ray photoelectron spectroscopy (XPS), electron microscopy (SEM and TEM), elemental microanalysis (EDS), infrared spectroscopy (FTIR), and thermal analysis (TGA and DTA). The XRD analysis revealed a well crystallized hydroxyapatite (HAp) structure at all temperatures. At 1000°C a small amount of CaO (about 1.2 %) was detected. The average crystallite size increased from 19 nm at 80°C to about 125 nm at 1000°C. FTIR spectra showed the presence of various  $PO_4^{3-}$  and  $OH^-$  groups present in the powders. In order to verify the biocompatibility of HAP powders with hFOB 1.19 osteoblasts cells, an 3-(4,5-dimethylthiazol-2-yl)-2,5-diphenyltetrazolium bromide (MTT) test was applied. It was noticed that the ceramics obtained at 1000°C, increased the cell viability with 10%, 40% and 55% after 6, 12 respectively 24 h, whereas that obtained at 600 °C was less effective. Our results proved the high biocompatibility of calcium phosphate ceramic powders obtained by sol-gel and sintered at 1000°C.

(Received October 10, 2010; accepted November 2, 2010)

*Keywords:* hydroxyapatite, nanoparticles, sol-gel, biocompatibility, cell viability, XRD, FTIR, TEM, SEM, EDS,

### 1. Introduction

Hydroxyapatite (HAp), with the structural formula of  $Ca_{10}(PO_4)_6(OH)_2$  is the principal inorganic constituent of human bones and teeth [1]. Synthetic HAP crystals are now widely used in medical applications e.g. as implants or coatings on prostheses. The biological characteristics as non-immunogenicity, non-inflammatory behavior, good biocompatibility, high osteoconductivity and/or osteoinductivity [2] of these synthetic HAP have been extensively studied.

It was revealed that in deproteinated bone the individual 25-50 nm HAP crystals are the essence of bone in terms of mechanical properties and bioresorbability and that they play an important role in biomineral formation [3].

The nano-sized HAP particles (nano HAp) raised a great interest and large efforts have been dedicated in the last two decades to study their synthesis, structure and properties. These

---

\*Corresponding author: dpredoi68@gmail.com

nano-HAPs have peculiar characteristics such as improved biocompatibility, good bioactivity and flexible structure which are important for their potential applications in medicine [1].

HAP has the ability to interact chemically with bone both in vitro and in vivo [4]. Significant amount of research on HAP has been devoted to its mechanical properties and on the hydroxyl ions ( $\text{OH}^-$ ) located at the centre of  $\text{Ca}^{2+}$  triangles along the c-axes of the hexagonal unit cell [5]. The  $\text{OH}^-$  ions are aligned in columns parallel to the c-axis along with  $\text{Ca}^{2+}$  and  $(\text{PO}_4^{3-})$  ions [6]. Since the  $\text{OH}^-$  ions within the c-axis columns are thought to have an important role in ionic conduction [5], HAP has been regarded as a one-dimensional anionic conductor [7].

Despite the chemical resemblance to the mineral component of bone, the peculiar brittleness and low fracture toughness of HAP has restricted its usage in applications such as high load-bearing implants [8]. Many methods for synthesis of HAP have been reported such as solid-state reaction, sol-gel, wet synthesis and hydrothermal methods. The key factors for getting controllable aspect ratios and bioactivity are: the reaction temperature, pH and concentration of reactants. The properties of HAP, in particular those mentioned above affects the efficiency of the powder in its ultimate applications [9].

Used as coating for some protease, it improves the healing duration and the quality of the body acceptance. It is useful to determine, as much as possible, its mechanical, bio-compatibility, chemical and physical properties. Considerable efforts were made to improve the mechanical properties of HAP by composite formation. The HAp nanoparticles are currently being tested as delivery vehicles in various medical applications that include delivery of growth factors, antibiotics, anticancer drugs, enzymes and antigens for slow release vaccination [10].

The surface properties of biomaterials are associated with cell adhesion and subsequent various cell behaviors such as proliferations, migration, cytoskeletal arrangement, and apoptosis [11].

Cell adhesion and its performance depend on the characteristics of substrates including chemical composition, surface charge, water wettability, roughness and size of cytophilic area [11]. In the field of biomaterials for substitution and reorganization of hard tissue, calcium phosphate ceramics are quite important because natural hard tissue is primarily composed as was mentioned above of HAP.

The composition, physico-chemical properties, crystal size and morphology of synthetic apatite are extremely sensitive to preparative conditions and sometimes results non-stoichiometric calcium deficient HAP powders.

The present paper describes the synthesis of calcium phosphate ceramics powders via sol-gel method, and the physical-chemical properties of HAP after calcinations at 600 and 1000°C. X-ray diffraction (XRD) and scanning electron microscopy with energy dispersive spectrometry attachment (SEM-EDS) were used for evaluation of the elemental and phase composition, grain and crystallite size, and morphology of the samples. For further support of the XRD analysis, we used TEM to observe the structure of the samples. The functional groups of the coatings were analyzed using Fourier transform infrared spectroscopy (FTIR).

The biocompatibility of HAPs calcined at 600 and 1000°C, was assessed through cell viability, morphology, and cytoskeleton analysis.

## 2. Powder preparation

The Hap ceramic powder was prepared (Ca/P molar ratio: 1.67) using  $\text{Ca}(\text{NO}_3)_2 \cdot 4\text{H}_2\text{O}$  and  $\text{P}_2\text{O}_5$  by a simple sol-gel approach. A designed amount of phosphoric pentoxide ( $\text{P}_2\text{O}_5$ , Merck) was dissolved in absolute ethanol to form a 0.5 mol/l solution. A designed amount of calcium nitrate tetrahydrate was also dissolved in absolute ethanol to form a 1.67 mol/l solution [12-13]. The mixture was stirred constantly for 24 h by a mechanical stirrer, allowing the reaction to complete at 80°C. A transparent gel was obtained. The gel was dried at 80°C for 96 h (HAp\_80) in an electrical air oven. The dried gels were individually heated at a rate of 5°C/min up to 600°C (HAp\_600) and 1000°C (HAp\_1000) for 6h. The sintered powders were ball milled at 100 rpm to get fine powders. The steps of obtaining by sol-gel method for hydroxyapatite is shown in Figure 1.

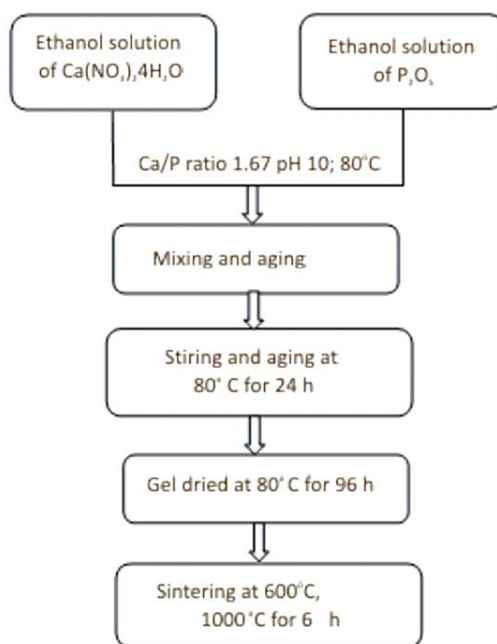


Fig. 1. The steps of obtaining by sol-gel method for Hap samples.

### 3. Powder characterization

**X-ray diffraction (XRD).** The samples were characterized for qualitative and quantitative phase content by X-ray diffraction (XRD) by using a Bruker D8-Advance X-ray diffractometer, in powder setting, equipped with a LynxEye type linear detector, using non-monochromatized  $\text{CuK}\alpha$  radiation, in the scanning range  $2\theta = 15 - 140^\circ$ . The qualitative phase analysis was performed with the EVA software package and ICDD- PDF-2- database For quantitative phase analysis the TOPAS software [14] was used with crystal structure data from the ICSD database [15].

**Scanning electron microscopy (SEM-EDS).** The structure and morphology of the samples were studied using a HITACHI S2600N-type scanning electron microscope (SEM), operating at 25kV in vacuum. The SEM studies were performed on powder samples. For the elemental analysis the electron microscope was equipped with an energy dispersive X-ray attachment (EDAX/2001 device).

**Transmission electron microscopy (TEM)** studies were carried out using Technai 120keV from FEI to precise the evolution of HAP with the thermal treatment. Classic modes such bright field (BF) to image the texture of the materials (shape, dimension) and Selected Area Diffraction (SAD) to precise the structure (crystallographic parameters) were used. The samples were prepared using ultramicrotomy to obtain thin samples with a thickness inferior to 80 nm. The preparations were deposited on a copper grid covered by a thin film of amorphous carbon. This protocol has been used in order to minimize sample artefacts such amorphization or preferential ablation induced by FIB for example or by ionic ablation [14].

**Thermal analysis.** The thermal behaviour of the powders was studied by differential thermal analysis (DTA) and thermal gravimetric analysis (TGA) using a Shimadzu DTG-TA-50 and DTA 50 analyzer in the 25-800°C temperature range, air environment, and  $\text{Al}_2\text{O}_3$  reference.

**FT-IR spectroscopy.** The functional groups present in the prepared powder and in the powders calcined at different temperatures were identified by FTIR (Spectrum BX Spectrometer). For this 1% of the powder was mixed and ground with 99% KBr. Tablets of 10 mm diameter for FTIR measurements were prepared by pressing the powder mixture at a load of 5 tons for 2 min and the spectrum was taken in the range of 400 to 4000  $\text{cm}^{-1}$  with resolution 4 and 128 times scanning.

**X-ray Photoelectron Spectroscopy (XPS)** is one of the most important techniques for the study of the elemental ratios in the surface region. The surface sensitivity (typically 40-100 Å) makes this technique ideal for measurements as oxidation states or biomaterials powder. In this analysis we have used a VG ESCA 3 MK II XPS installation ( $E(Al_{k\alpha})=1486.7$  eV). The vacuum analysis chamber pressure was  $p \sim 3 \times 10^{-8}$  torr. The XPS recorded spectrum involved an energy window  $w=20$  eV with the resolution  $R= 50$  eV with 256 recording channels. The XPS spectra were processed using Spectral Data Processor v2.3 (SDP) software.

#### **Cell culture**

The hFOB 1.19 osteoblasts cells line was purchased from ATCC (American Type Culture Collection) and maintained in DMEM, containing 3,7 g/L sodium bicarbonate, 4,5g/L D-glucose, 4,7g/L HEPES, 4 mM L-glutamine, 0,1 mM sodium pyruvate, 100 U/ml penicillin, 100 U/ml streptomycin and 10% (v/v) fetal bovine serum. Cells were grown in 5% CO<sub>2</sub> at 37°C and plated at  $5 \times 10^4$  cells/cm<sup>2</sup> in Ø 100 mm culture dishes with a medium change twice a week. When 70-80% confluence was reached, cells were passaged and hFOB 1.19 cells prior to passage 4 were used in this study.

The HAp ceramic discs with dimensions of 10 mm Ø x 10 mm were rinsed in distilled water and autoclaved at 125°C/0.14 MPa for 60 min.

Cells cultured in dishes prior to passage 3 were detached by treatment with trypsin-EDTA (0.25% and 0.03% respectively) and loaded on HAp ceramic discs at a seeding density of  $5 \times 10^4$  cells/cm<sup>2</sup> in 24-well plates. Cells cultured in 24-well plates at the same seeding density were used as control.

#### **Cell viability**

The viability of the cells was determined by the tetrazolium salt test [16]. The medium from each well was removed by aspiration, the cells were washed with 200 µl phosphate buffer solution (PBS)/well and then 50µl (1mg/mL) of 3-(4,5-dimethylthiazol-2-yl)-2,5-diphenyltetrazolium bromide (MTT) solution was added on each well. After 2 hours of incubation the MTT solution from each well was removed by aspiration. A volume of 50 µl isopropanol was added and the plate was shaken to dissolve the formazan crystals. The optical density at 595nm, for each well, was then determined using a Tecan multiplate reader (Tecan GENios, Grödic, Germany). The absorbance from the wells of cells cultured in the absence of ceramic discs was used as the 100% viability value.

#### **Cell morphology**

The cells were plated at day one at a density of  $5 \times 10^4$  cells/cm<sup>2</sup> on the ceramics discs. At specific time points cells were imaged by a bright field inverted microscope (Olympus IX7). Images were acquired by specific software Cell F using a CCD video camera COLORVIEW

#### **Analysis of the $\alpha$ -tubulin cytoskeleton**

The hFOB 1.19 cells were cultured on the discs for 24 hours and fixed with 4% paraformaldehyde in PBS for 15-20 minutes, followed by three washes of 10 minutes with PBS. Subsequently, a treatment with 2% BSA in PBS and 0.1% Triton X-100 was done for one hour at room temperature, followed by three washes with PBS. The cells on discs were incubated with mouse primary antibody against  $\alpha$ -tubulin (Santa Cruz) diluted 1:50 in 1.2% BSA in PBS for 2 hours at room temperature, followed by three washes of 10 minutes with PBS. Then the 1:100 diluted secondary antibody coupled with biotin was added and finally FITC coupled streptavidin diluted 1:60 was applied for one hour in dark. The cells were analyzed at an Olympus IX71 microscope using an excitation wavelength of 495 nm and an emission one of 513nm.

## **4. Results and discussion**

The micro-structure of the ceramic powders prepared by sol-gel synthesis is strongly affected by the sintering temperature [13]. Figure 2 shows the XRD patterns of the powders obtained at 80, 600 and 1000°C. There are displayed also the characteristic diffraction lines of a standard HAp powder according to ICDD-PDF2 card no 9-432, with the Miller indices corresponding to the most intensive peaks. Beside hydroxylapatite, a small amount of CaO was identified in the powder treated at 1000°C. The presence of CaO after heat treatment is in agreement with the results reported by Kutty [17] and Skinner et al [18]. With the increase of the

calcination temperature HAp would have started losing hydroxyl groups forming various phosphates. The proposed reaction is [13]:



The  $\text{Ca}_3(\text{PO}_4)_2$  phase can not be seen in the XRD pattern of the sample annealed at  $1000^\circ\text{C}$ ; just a slight shoulder on the left hand side of HAp (211) peak can suggest its presence as  $\beta\text{-Ca}_3(\text{PO}_4)_2$ . In Figure 2 one can observe also that the HAp peaks become narrower as the sintering temperature increases from  $80$  to  $1000^\circ\text{C}$ , indicating an increase of the crystallite size. However between the patterns of the dried sample and of that treated at  $600^\circ\text{C}$  only very slight differences can be noticed by visual inspection. In order to determine both the percent of the additional phases, and the average crystallite size of hydroxylapatite, the diffraction data were processed by Rietveld whole powder pattern fitting, using TOPAS 3. The peak shapes and widths were calculated by the fundamental parameters approach [19], after a calibration of the physical parameters of the diffractometer by using a corundum reference sample (NIST SRM 1976). The average crystallite size was determined assuming isotropic crystallite shapes and neglecting lattice strains. The unit cell structures of the component phases were restricted in what concerns atomic sites, occupancies and temperature factors to ICSD # 99358 for hydroxylapatite, to ICSD # 90486 for lime, and to ICSD # 97500 for  $\beta\text{-Ca}_3(\text{PO}_4)_2$ . A good fit was obtained, especially for the sample annealed at  $1000^\circ\text{C}$ . For  $80^\circ\text{C}$  and  $600^\circ\text{C}$  systematic discrepancies were noticed between the experimental and simulated line shapes corresponding to the (00 $l$ ) crystalline planes of HAp. This is believed to be related to the anisotropic crystallite size of HAp at lower temperatures revealed by the TEM images that is elongated crystallites along the crystallographic  $c$  axis. The following results were obtained for the mean crystallite sizes:  $D = 18.7 (\pm 0.1)$  at  $80^\circ\text{C}$ ,  $D = 28.7 (\pm 0.7)$  nm at  $600^\circ\text{C}$  and  $D = 125 (\pm 2)$  nm at  $1000^\circ\text{C}$ . The concentrations of minor phases occurred after thermal treatment at  $1000^\circ\text{C}$  resulted as: 1.2 wt % CaO and 0.2 wt%  $\beta\text{-Ca}_3(\text{PO}_4)_2$ . One can expect large errors because of the weak intensities of the (hypothetical)  $\beta\text{-Ca}_3(\text{PO}_4)_2$  phase and because of the overlaps of its peaks with the HAp peaks.

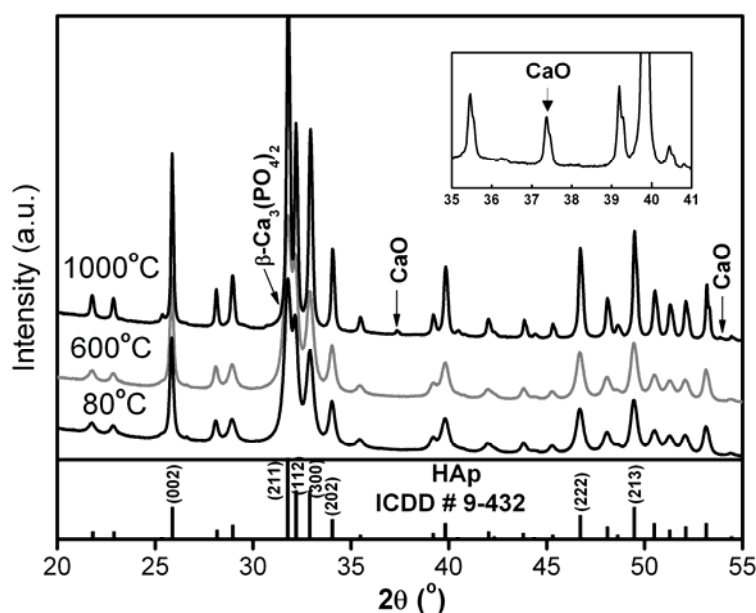


Fig. 2. The X-ray diffraction patterns of the powder after heat treatment at  $80^\circ\text{C}$ ,  $600^\circ\text{C}$  and  $1000^\circ\text{C}$

The composition of the nano-sized HAp powders prepared by sol-gel method was analyzed by energy dispersive X-ray spectroscopy (EDS). Figure 2D shows the EDS spectrum of the HAp

powders. The composition analysis by EDS shows that the Ca/P ratio in the samples is 1.67 which is similar to the theoretical value in HAp.

The effect of the post-treatment temperature on the morphology and crystal structures of the powder was investigated. The gels were dried at 80°C for 96h and the resulting powders were post-treated at 600 and 1000°C. The Figure 3 A-C shows the SEM photograph of the post-treated powder (80°C, 600°C and 1000°C). It can be seen that the HAp morphology is dependent of the heat treatment.

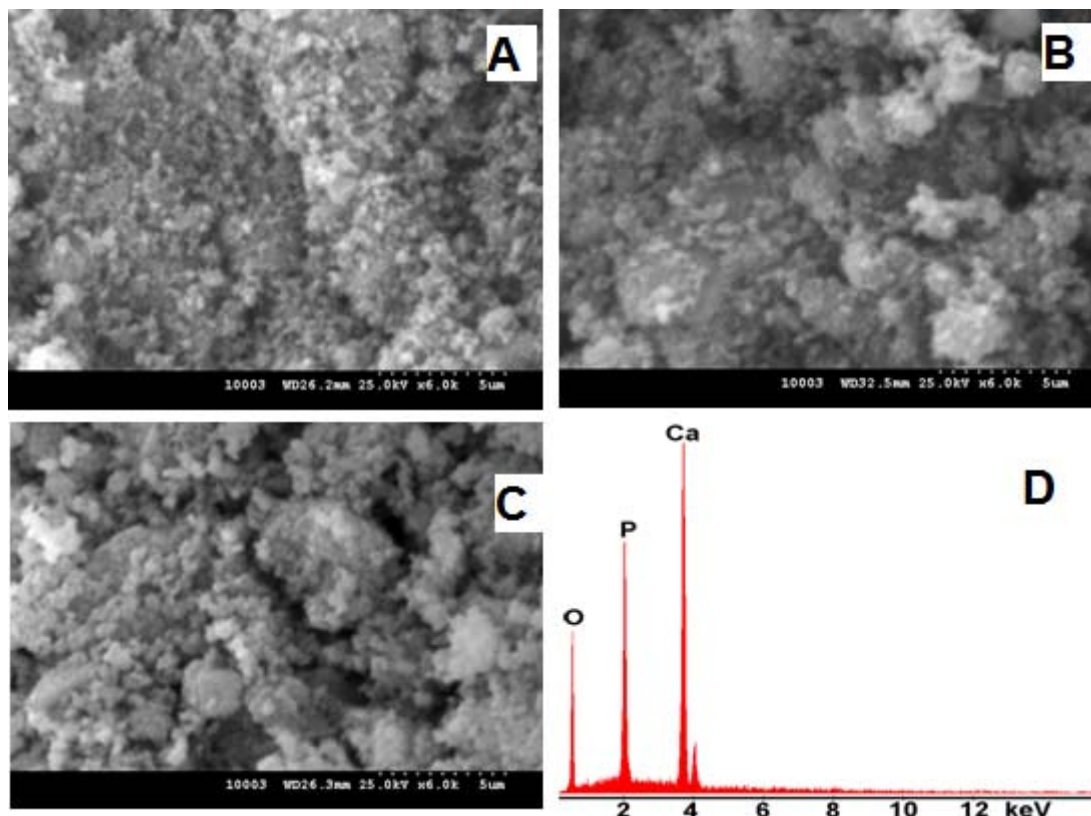


Fig. 3. Typical SEM images of the powders obtained at 80°C (A) and after heat-treatment at 600°C (B) and 1000°C (C). EDS spectra of the powder obtained at 80°C (D).

TEM micrography of HAp at 80°C, 600°C and 1000°C (respectively Figure 4A, B and C) clearly reveal the influence of heat treatment on the crystallography of the material. At 80°C, HAp appear on BF and SAD (Figure 4A) respectively poorly crystallized with flowing shape and about 0,1µm size; SAD pattern is typical of Debye-Scherrer one with large ring and some large bright points. This trend reflects a poor stage of crystallization. Typically rings of higher diffraction angles are not well defined with weak bright point close to the diffusion beam or missing. At 800°C (Figure 4B), the crystals (size and shape) do not reveal any evident difference compare to HAp at 80°C. Only the SAD shows some rings thinner with small bright points, traducing a better crystallization state: larger single crystal with less default than at 80°C. Finally, samples cured at 1000°C exhibits large hexagonal crystals with SAD reflecting a hexagonal cell and doted of well defined bright points typical of large single crystals diffracting the electron beam. Comparing this result with the average crystallite size determined by XRD (125 nm), one can conclude that these “crystals” represent agglomerations of thousands of crystallites (coherence domains).

The decomposition temperature strongly depends on the synthesis technique of the HAp powder. The TGA and DTA curves of the hydroxyapatite dried at 80°C are shown in Figure 5. The total mass loss in the heat-treatment process is about 5.84 %. A relatively pronounced mass loss occurs between 25 and 300°C, with the associated endothermic peak attributed to adsorbed water. The dominating weight loss occurred between 300 and 800°C corresponds to the evaporation, desorption and burning of the residual EtOH solvent. The decomposition of carbonate into CO<sub>2</sub>

gas occurred from 600 to 800°C [20]. From 800°C to 1300°C, a slight decrease in TGA curves shows the decomposition of  $\text{Ca}_{10}(\text{PO}_4)_6$  in  $\text{CaO}$  and  $\text{Ca}_3(\text{PO}_4)_2$ . This result is in good agreement with the occurrence of  $\text{CaO}$  lines in the XRD patterns at 1000°C.

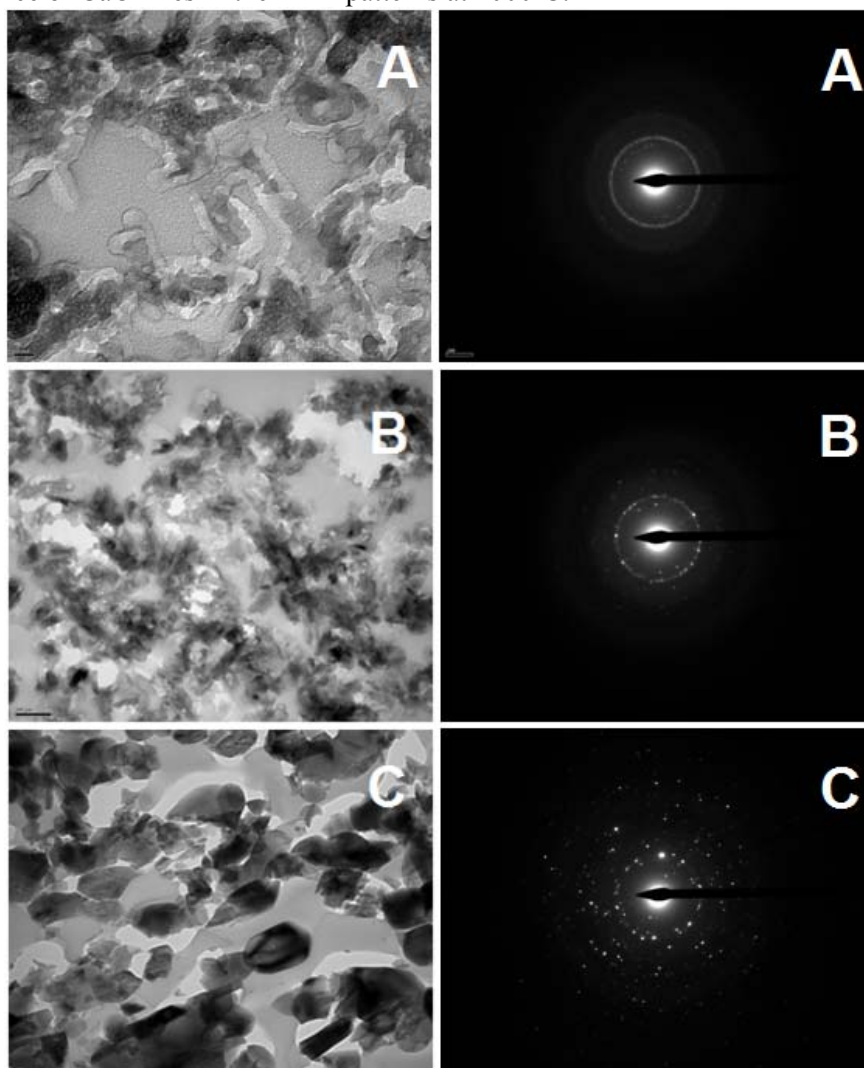


Fig. 4. Micrographs (BF and SAD) of HAp at 80°C (A), 600°C (B) and 1000°C (C).  
on the images A, B, C the magnification bars must be displayed

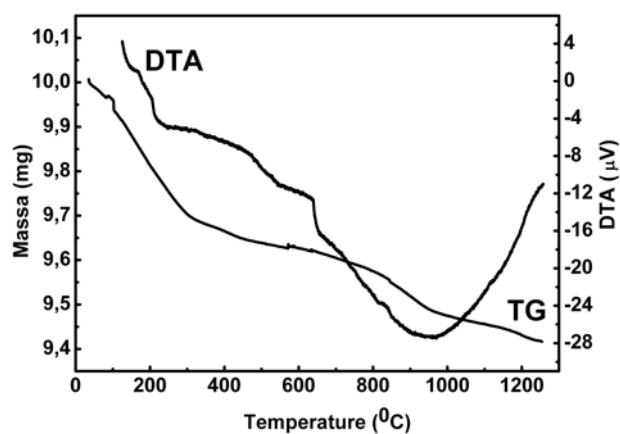


Fig. 5. DTA and TG curves of the gel dried at 80°C  
(recording at a heating rate of 10 °C/min in air)

Figure 6A shows FT-IR spectra of the HAp at 80°C, and heated at 600°C and 1000°C. The wave number of bands and their assignments are summarized in Table 1. The fundamental vibration modes of  $\text{PO}_4^{3-}$ ,  $\nu_1$ ,  $\nu_2$ ,  $\nu_3$  and  $\nu_4$ , are observed. FTIR spectra (Figure 6B and Figure 6C) indicate that all the samples exhibit the characteristic bands of phosphate groups of the apatitic structure at about 470  $\text{cm}^{-1}$  ( $\nu_2$ ), 550 and 600  $\text{cm}^{-1}$  ( $\nu_4$ ), 960  $\text{cm}^{-1}$  ( $\nu_1$ ) and 1020-1120  $\text{cm}^{-1}$  ( $\nu_3$ ) [21-24]. The band at 1400  $\text{cm}^{-1}$  was attributed to residual  $\text{NO}_3^-$  groups resulting from synthesis precursors. The band at 860  $\text{cm}^{-1}$  is associated with  $\nu_2$  vibrations of carbonate groups, and at 1470  $\text{cm}^{-1}$  is associated with  $\nu_3$  vibrations carbonate groups [25].  $\text{CO}_3^{2-}$  and  $\text{NO}_3^-$  are the common impurities in the HAp synthesis. The intensities of both  $\text{CO}_3^{2-}$  and  $\text{NO}_3^-$  peaks decreased at higher calcinations temperatures because they are released as volatile gases (Figure 6C). The spectrum of HAp had characteristic bands at 632 and 3572  $\text{cm}^{-1}$ , corresponding to O-H groups located in the apatite channels (Figures 6B, 6C and 6D) [26]. The pronounced hydroxyl bands at 632 and 3572  $\text{cm}^{-1}$  are typical of hydroxyapatite with a high degree of crystallinity, powder sintered at high temperature [27]. The broad bands in the regions 1600-1700  $\text{cm}^{-1}$  and 3200-3600  $\text{cm}^{-1}$  correspond to H-O-H bands of lattice water [28-29]. In all the spectra of the samples heated, the intensity of the large bands which was attributable to adsorbed water diminished (Figures 6C and 6D).

Table 1: Characteristic wave number of powder HAp at 80°C and sintered at 600°C and 1000°C

Samples			Assignment
HAp 80	HAp 600	HAp 1000	
470	470	470	$\nu_2(\text{PO}_4^{3-})$
550	550	550	$\nu_4(\text{PO}_4^{3-})$
600	600	600	$\nu_4(\text{PO}_4^{3-})$
632	632	632	$\nu_L(\text{OH}^-)$
860	860	860	$\nu_2(\text{CO}_3^{2-})$
960	960	960	$\nu_1(\text{PO}_4^{3-})$
1040	1040	1040	$\nu_3(\text{PO}_4^{3-})$
1100	1100	1100	$\nu_3(\text{PO}_4^{3-})$
1400	1400	1400	$\nu(\text{NO}_3^{2-})$
1470	1470	1470	$\nu_3(\text{CO}_3^{2-})$
1640	1640	1640	$\nu(\text{OH}^-)$ adsorbed water
3450	3450	3450	$\nu(\text{OH}^-)$ adsorbed water
3572	3572	3572	$\nu_3(\text{OH}^-)$

In order to evaluate the degree of compatibility of HAp 80 HAp 600 and HAp 1000 with hFOB 1.19 osteoblasts cells, the MTT test for short term (6, 12 and 24 hours) was performed in order to explore the cellular interaction with the nanostructured surface. In Figure 6 these results are presented. As it can be seen, the cells cultivated on HAp 80 revealed the lowest the viability.

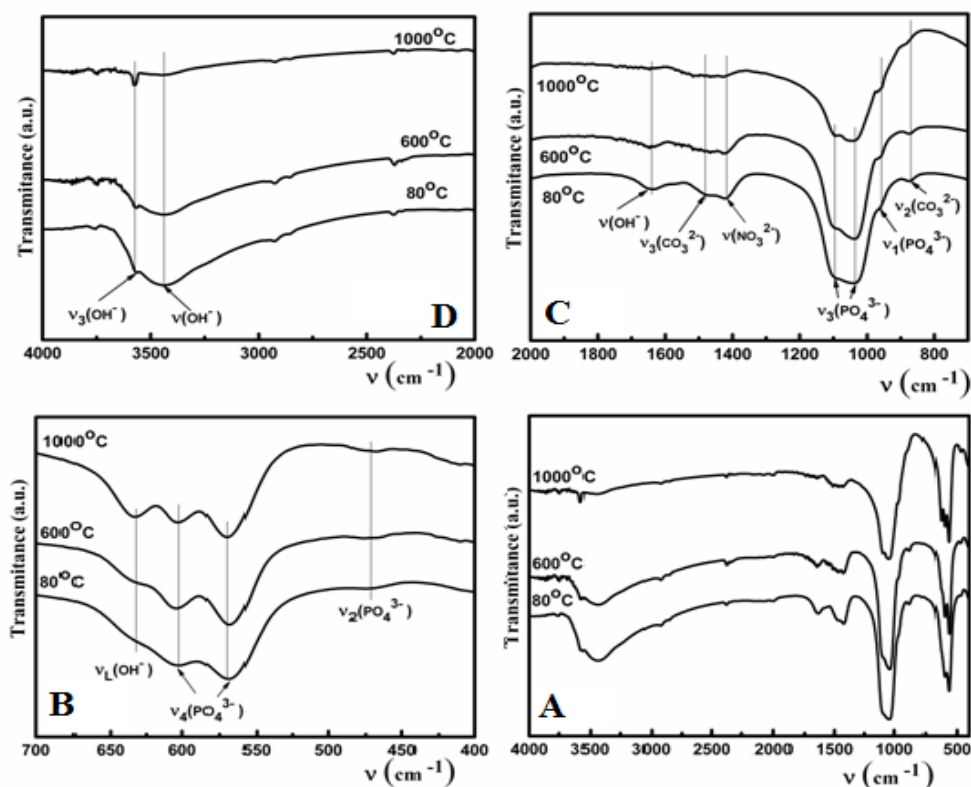


Fig. 6. The FT-IR spectra of powder obtained at 80°C and after heat-treatment at 600°C (HAp\_600) and 1000°C (HAp\_1000).

A representative survey spectrum for hydroxyapatite powder obtained at 80°C (Hap\_80) is presented in Figure 7 together with the expected positions of the main lines (Ca 2p at 347.10 eV, O1s at 531 eV and P 2p at 133.8 eV respectively). For XPS analysis the binding energies were calibrated with reference to C 1s at 285 eV. The Ca(2p) signal is composed of two lines Ca 2p<sub>1/2</sub> (350.67eV) dedicated to calcium apatite and Ca 2p<sub>3/2</sub> (347.13 eV) relate to a simple Ca-O bond. As a general observation the ratio Ca/P is nearly stoichiometric. The SDP deconvoluted spectra for O, Ca and P are presented (Figure 8).

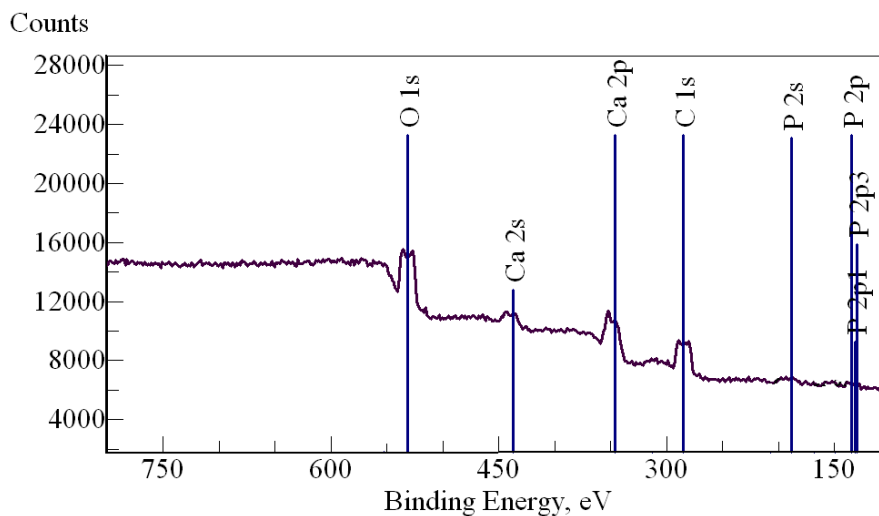


Fig. 7. XPS spectrum of the HA\_80 sample.

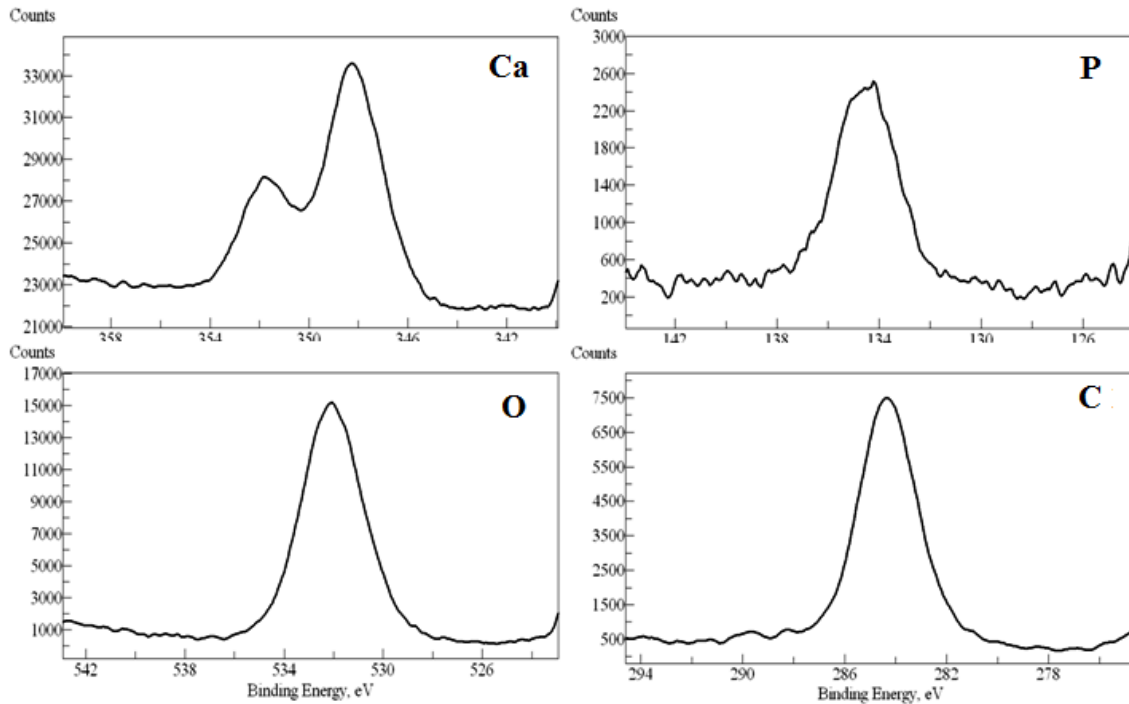


Fig. 8. XPS spectra for Ca, P, O and C are presented

On the other hand, the osteoblasts cultivated on the other three ceramics types were good compared to control (Figure 9). Whereas HAp 600 induced an increase of viability of only 5.3% and 19.4% after 12 respectively 24h but the highest level of viability was noticed for HAp\_1000, with 10.2%, 23.5% and 56.4% after 6, 12 respectively 24h. It is obvious that HAp 1000 stimulated the highest viability of hFOB 1.19 cells.

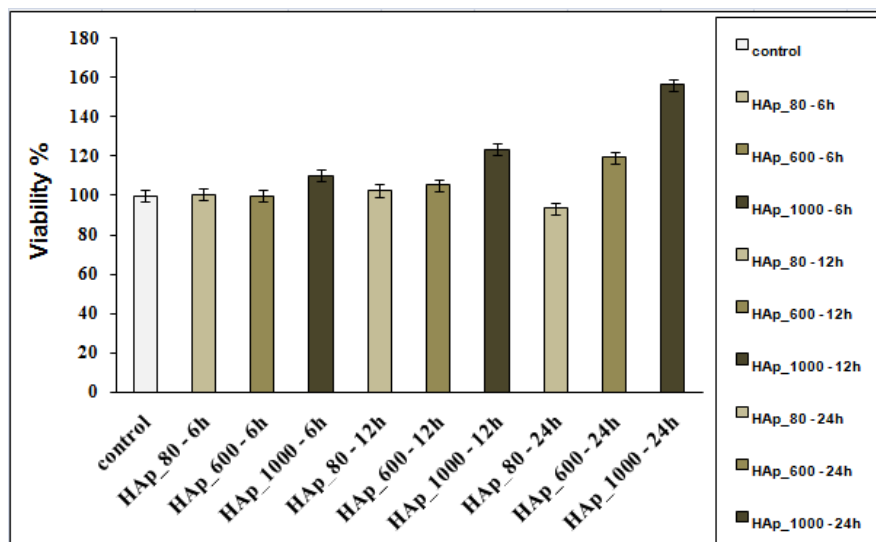


Fig. 9. The viability of hFOB 1.19 cells plated on HAp\_80, HAp\_600 and HAp\_1000 for 6, 12 and 24 hours.

None of the ceramics altered the cellular morphology in term of size and shape (Figure 10 top) is observed. On the all material types, no specific orientation of the centrosome and similar

extent of microtubules polymerization (Figure 10 down) were notice. According to Fig. 10, it can be seen that a layer of fusiform cells of osteoblast has been coated on the surface of the HAp samples.

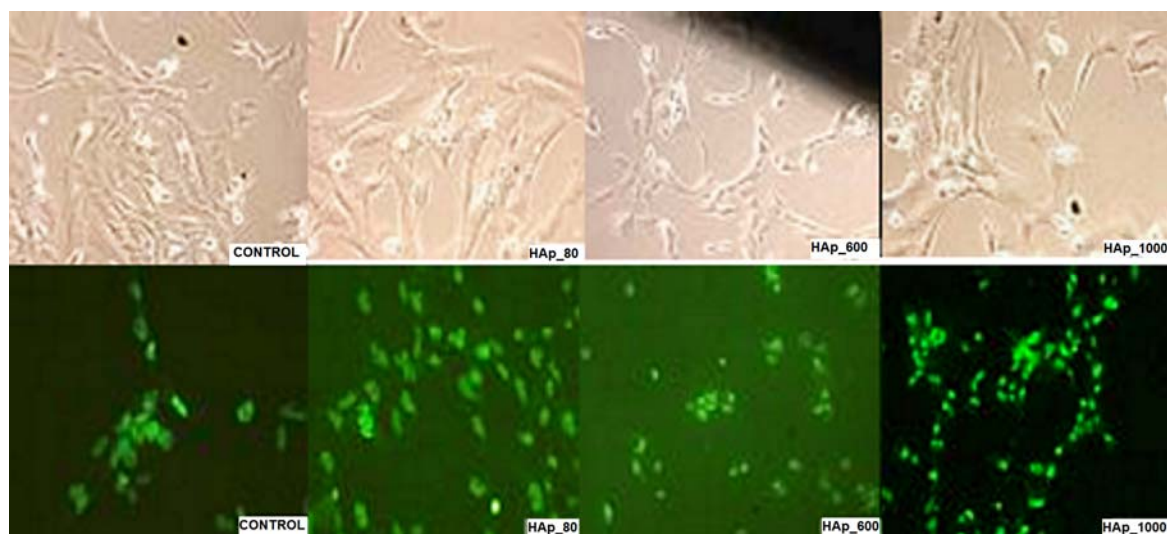


Fig. 10. Microscopical analysis of hFOB 1.19 cells plated on HAp\_80, HAp\_600 and HAp\_1000 for 24 hours; cell morphology (top), anti  $\alpha$ -tubulin staining (down).

The cytotoxicity of the samples is distinguished by development of layer of cells and also their fusiform morphology. Thus, the Hap samples were considered not toxic for hFOB 1.19 mouse osteoblast cells. Meaning that with regard to Figures 7, Hap\_80, Hap\_600 and Hap\_1000 samples did not show any sign of toxicity with hFOB 1.19 cells.

## 5. Conclusions

The sol-gel method provides a simple route for synthesis of hydroxyapatite nanopowder. The crystallinity and morphology of the obtained nanopowder depend on the sintering temperature. The effects of high temperature treatments of the gels on the morphology, grain and crystallite size of the nano-sized HAp powders were investigated. The characteristic FTIR peaks of different groups corresponding to residuals and resulted materials were identified in detail. TEM revealed elongated (nano-sized) grains at lower temperatures, which become micrometric and almost spherical after heat treatment at 1000°C, while XRD gave nano-sized crystallites at all temperatures, elongated along the  $c$  axis at low temperatures. A small amount of CaO has been found after heat treatment at 1000°C showing that HAp starts to thermally decompose at this temperature.

All nanocomposites are suitable substrates for adherence and cell proliferation, but HAp\_1000 is the best support. It is important to conclude that HAp\_600, and HAp\_1000 bioceramics have micro cells configurations that allow them to be used for obtaining medical biocompatible supports. The cell proliferation is similar to the control for all the samples. The excellent results were obtained only in the case of Hap\_1000 sample.

Heat-treated nano-particles are in favor of the adhesion of cells. Therefore, nano-particles materials are greatly promising in the development of more valuable orthopedic and dental implants. However the mechanism of nano-HAp/osteoblast interaction is expected to investigate thoroughly, which will promote the research of biomaterials with better biological performance.

### Acknowledgements

This work was financially supported by Science and Technology Ministry of Romania (PNCDI II 71-097/2007 and Core Program contract PN09-45).

### References

- [1] Zhangli Shi, Xin Huang, Yurong Cai, Riukang Tang, Disheng Yang, *Acta Biomaterialia* **5**, 338 (2009)
- [2] Hornez J.C., Chai F., Manchau F., Blanchemain N., Descampes H., Hildebrand H.F., *Biomol Eng.* **24**(5), 505 (2007).
- [3] S. Zhang, Y.S. Wang, X.T. Zeng, K. Cheng, M. Qian, D.E. Sun, W.J. Weng, W.Y. Chia, *Engineering Fracture Mechanics*, **74**(12), 1884 (2007).
- [4] J.P. Gittings, C.R. Bowen, A.C.E. Dent, I.G. Turner, *Acta Biomaterialia* **5**, 743 (2009)
- [5] Yamashita K., Kitagoki K., Umegaki T., *J. Am. Ceram. Sec.* **78**, 1191 (1995)
- [6] Mahabele M.P., Aiyer R.C., Ramakrishna C.V., Sreedhar B., Khairnar R.S., *Bull. Mater Sci.* **28**, 535 (2005).
- [7] Yamashita K., Owada H., Umegaki T., Kasazawa T., Futagamu T., *Solid State Ionics* **60**, 660 (1988).
- [8] G.B. Warren, J. C. Metcalfe, A.G. Lee, N. J.M. Birdsall, *FEBS Letters*, **50**(2), 261 (1975)
- [9] Chandrasekhar Kothapalli, M. Wei, A. Vasiliev, M.T. Shaw, *Acta Materialia* **52**, 5655 (2004).
- [10] M. Motskin, D.M. Wright, K. Muller, N. Kyle, T.G. Gard, A.E. Porter, J.N. Skepper, *Biomaterials* **30**, 3307-3317, (2009).
- [11] Shinnosuke Okada, Hiroyuri Ito, Atsushi Nagai, Jun Komotori, Hiroaki Imai, *Acta Biomaterialia* **6**, 591-597, (2010)
- [12] M. H. Fathi, A. Hanifi, *Materials Letters* **61**, 3978, (2007)
- [13] D.Predoi, R.A. Vatasescu-Balcan, I. Pasuk, R. Trusca, M. Costache, *Journal of Optoelectronics and Advanced Materials*, **10**(8), 2151 (2008)
- [14] Bruker AXS: *TOPAS V3*: General profile and structure analysis software for powder diffraction data. - User's Manual, Bruker AXS, Karlsruhe, Germany, (2005)
- [15] Inorganic Crystal Structure Database©, Fachinformationszentrum Karlsruhe, Germany, and the U.S. Department of Commerce, United States, (2005)
- [16] J. Mosmann, *J Immunol Methods* **65**, 55 (1983)
- [17] T.R.N. Kutty, *Indian J. Chem.* **11**, 695 (1973)
- [18] H.C.W. Skinner, J.S. Kittelbergen, R.A. Beebe, *J. Phys. Chem.* **79**, 2017 (1975)
- [19] R. W. Cheary, A. A. Coelho, *J. Appl. Cryst.* **25**, 109 (1992)
- [20] R. Ganguly, V. Siruguri, I.K. Gopalakrishnan, J.V. Yakhmi, *Journal of Physics: Condensed Matter* **12**, 1683 (2000).
- [21] L. Bernard, M. Freche, J.L. Lacout, B. Biscans, *Phosphorus Res. Bull.* **10**, 364, (1999)
- [22] K.C. Blakeslee, R.A. Conrad Sr, *J. Am Ceram. Soc.* **54**, 559, (1971)
- [23] S.J. Joris, C.H. Amberg, *J. Phys. Chem.* **75**, 3172, (1971)
- [24] V.M. Bhatnagar, *Bull. Soc. Chem. Fr.* **8**, 1771, (1968)
- [25] C.C. Silva, H.H.B. Rocha, F.N.A. Freire, M.R.P. Santos, K.D.A. Saboia, J.C. Goes, A.S.B. Sombra, *Materials Chemistry and Physics* **92**, 260, (2005).
- [26] A. Bigi, E. Boanini, K. Rubini, *J. Solid. State. Chem.* **177**, 3092, (2004).
- [27] Z. Hong, L. Luan, S.B. Paik, B. Deng, D.E. Ellis, J.B. Ketterson, A. Mello, J.G. Eon, J. Terra, A. Rossi, *Thin Solid Films* **515**, 6773, (2007).
- [28] D. Predoi, R. V. Ghita, F. Ungureanu, C. C. Negrila, R. A. Vatasescu-Balcan, M. Costache, *J. Optoelectron. Adv. Mater.* **9**(12), 3827 (2007).
- [29] D. Predoi, M. Barsan, E. Andronescu, R.A. Vatasescu-Balcan and M. Costache, *J. Optoelectron. Adv. Mater.* **9**(11), 3609 (2007)